Manuscript prepared for Atmos. Chem. Phys. Discuss.
with version 2014/05/30 6.91 Copernicus papers of the LaTeX class copernicus.cls.
Date: 7 August 2014

Worldwide biogenic soil NO_x emissions inferred from OMI NO_2 observations

G. C. M. Vinken[1], K. F. Boersma[2,3], J. D. Maasakkers[1,*], M. Adon[4,5], and R. V. Martin[6,7]

[1]Department of Applied Physics, Eindhoven University of Technology, Eindhoven, the Netherlands
[2]Department of Meteorology and Air Quality, Wageningen University, Wageningen, the Netherlands
[3]Climate Observations Department, Royal Netherlands Meteorological Institute, De Bilt, the Netherlands
[4]Laboratoire d'Aérologie, UMR CNRS/UPS 5560, Toulouse, France
[5]Laboratoire de Physique de l'Atmosphère, Université Félix Houphouët-Boigny, Abidjan, Côte d'Ivoire
[6]Department of Physics and Atmospheric Science, Dalhousie University, Halifax, Nova Scotia, Canada
[7]Harvard-Smithsonian Center for Astrophysics, Cambridge, MA, USA
[*]now at: Department of Earth and Planetary Sciences, Harvard University, Cambridge, MA, USA

Correspondence to: G. C. M. Vinken (g.c.m.vinken@tue.nl)

Abstract

Biogenic NO_x emissions from soils are a large natural source with substantial uncertainties in global bottom-up estimates (ranging from ~~4 to 27~~ 4 to 15 Tg N yr^{-1}). We reduce this range in emission estimates, and present a top-down soil NO_x emission inventory for 2005 based on retrieved tropospheric NO_2 columns from the Ozone Monitoring Instrument (OMI). We use a state-of-science soil NO_x emission inventory (Hudman et al., 2012) as a priori in the GEOS-Chem chemistry transport model to identify 11 regions where tropospheric NO_2 columns are dominated by soil NO_x emissions. Strong correlations between soil NO_x emissions and simulated NO_2 columns indicate that spatial patterns in simulated NO_2 columns in these regions indeed reflect the underlying soil NO_x emissions. Subsequently, we use a mass-balance approach to constrain emissions for these 11 regions on all major continents using OMI observed and GEOS-Chem simulated tropospheric NO_2 columns. We find that responses of simulated NO_2 columns to changing NO_x emissions are suppressed over low NO_x regions, and account for these non-linearities in our inversion approach. In general, our approach suggests that emissions need to be increased in most regions. Our OMI top-down soil NO_x inventory amounts to 10.0 Tg N for 2005 when only constraining the 11 regions, and 12.9 Tg N when extrapolating the constraints globally. Substantial regional differences exist (ranging from −40 % to +90 %), and globally our top-down inventory is 4–35 % higher than the GEOS-Chem a priori (9.6 Tg N yr^{-1}). We evaluate NO_2 concentrations simulated with our new OMI top-down inventory against surface NO_2 measurements from monitoring stations in Africa, the USA, and Europe. Although this comparison is complicated by several factors, we find an encouraging improved agreement when using the OMI top-down inventory compared to using the a priori inventory. To our knowledge, this study provides, for the first time, specific constraints on soil NO_x emissions on all major continents using OMI NO_2 columns. Our results rule out the ~~high~~ low end of reported soil NO_x emission estimates, and suggest that global emissions are most likely around ~~10–13~~12.9±3.9 Tg N yr^{-1}.

1 Introduction

An important source of biogenic nitrogen oxide ($NO_x = NO + NO_2$) emissions is bacteria in soils. Nitrogen oxides play a key role in atmospheric chemistry by catalysing ozone (O_3) production. Tropospheric O_3 influences the hydroxyl-radical (OH) budget that determines the lifetime of reactive greenhouse gases (e.g. methane) (Steinkamp et al., 2009), thereby affecting the Earth's radiative balance (IPCC, 2007). Furthermore, NO_x emissions contribute to increased nitrogen deposition, which is important for soil NO_x emissions (via soil N content) (Hudman et al., 2012), and biomass burning NO_x emission factors (Castellanos et al., 2014). NO_x also leads to ammonium sulphate and nitrate particle formation in combination with ammonia (NH_3) emissions in rural areas (Zhang et al., 2012), and these particles are efficient in scattering sunlight back to space. The largest source of NO_x emissions is anthropogenic (21–28 $Tg\,N\,yr^{-1}$) (Denman et al., 2007), but estimates of natural emissions range from ~~12 to 47~~12 to 35 $Tg\,N\,yr^{-1}$. Natural sources include soil emissions (~~4–27~~ 4–15 $Tg\,N\,yr^{-1}$), biomass burning (6–12 $Tg\,N\,yr^{-1}$) and lightning (2–8 $Tg\,N\,yr^{-1}$) (Schumann and Huntrieser, 2007). The wide range in soil NO_x emission estimates reflects our incomplete knowledge of emission factors and processes driving these emissions. Reducing these substantial uncertainties will improve our understanding of tropospheric O_3 and aerosol burdens, and allow for a proper assessment of the impact of soil emissions on nitrogen deposition.

Soil NO_x is mainly emitted as NO, released as by-product of microbial nitrification ($NH_4^+ \rightarrow NO_3^-$) and denitrification ($NO_3^- \rightarrow N_2$) in soils (Firestone and Davidson, 1989; Conrad, 1996). Soil emissions are proportional to the amount of N cycled through these reactions, and correlated with N_2 and N_2O emissions (Parton et al., 2001). Furthermore, emissions strongly depend on climate and soil conditions like temperature, soil moisture, and soil N content (e.g. Ludwig et al., 2001; van Dijk et al., 2002; Stehfest and Bouwman, 2006, and references therein). Nearly 70 % of global soil emissions are emitted in the tropics (Yienger and Levy, 1995), and large pulses of biogenic NO emissions following the onset of rains after a dry period have been reported (e.g. Davidson, 1992; Scholes et al., 1997; Jaeglé et al., 2004; Bertram et al., 2005; Hudman et al., 2010). These pulsing events occur when water-stressed nitrifying bacteria,

which remain dormant during dry periods, are activated by the first rains and start metabolising accumulated inorganic N in the soil. This process releases NO pulses of up to 10–100 times the background levels, and lasts for about 1–2 days (Yienger and Levy, 1995; Hudman et al., 2012, and references therein). Numerous studies furthermore showed that application of fertiliser (using either ammonium or nitrate) results in large increases in soil NO_x emissions (e.g. Williams et al., 1988; Shepherd et al., 1991). Part of the applied fertiliser will be lost as NO, with fractions ranging from 0.55 % to 2.5 % (Yienger and Levy, 1995; Bouwman et al., 2002; Stehfest and Bouwman, 2006). Stehfest and Bouwman (2006) estimated total annual soil NO_x emissions from agriculture at 1.6 $Tg\,N\,yr^{-1}$.

Soil NO_x emissions have been estimated previously by process-based models (Potter et al., 1996; Parton et al., 2001), scaling field observations (Davidson and Kingerlee, 1997), and semi-empirical models (Yienger and Levy, 1995; Steinkamp and Lawrence, 2011; Hudman et al., 2012). With the exception of one study, total soil NO_x emissions of these models are between ~~4 and 27~~ 4 and 15 $Tg\,N\,yr^{-1}$, with large uncertainties of up to 5–10 $Tg\,N\,yr^{-1}$ (Davidson and Kingerlee, 1997). Part of the uncertainty in (above-canopy) soil NO_x emissions results from accounting for loss of soil NO_x emissions to plant canopy (Jacob and Bakwin, 1991; Ganzeveld et al., 2002b). Many chemistry transport models (CTMs) still use the semi-empirical soil NO_x model developed by Yienger and Levy (1995), which results in above-canopy global soil NO_x emissions of 5.5–6.2 $Tg\,N\,yr^{-1}$ (Wang et al., 1998). Recently, Steinkamp and Lawrence (2011) have updated the Yienger and Levy (1995) model, introducing a new biome type land-cover map and improved emission factors, resulting in an above-canopy estimate of 8.6 $Tg\,N\,yr^{-1}$ using a geometric mean of field measurements of emission factors (and 26.7 $Tg\,N\,yr^{-1}$ when using an arithmetic mean). Hudman et al. (2012) further improved the Steinkamp and Lawrence (2011) model by including a more physical parameterisation that takes into account the pulsing, soil moisture, and temperature dependence. This resulted in above-canopy global soil NO_x emissions of 9.0 $Tg\,N\,yr^{-1}$. A summary of soil NO_x estimates found in literature is given in Fig. 1.

Various sources of NO_x emissions have been constrained in the past using satellite observations of NO_2 columns (e.g. Martin et al., 2003). More recent studies have used the Ozone

Monitoring Instrument (OMI) to constrain (all) global NO_x emissions (e.g. Miyazaki et al., 2012; Stavrakou et al., 2013), or regional NO_x emissions over China (e.g. Lin et al., 2010). Jaeglé et al. (2005) derived a global soil NO_x emissions total of 8.9 $Tg\,N\,yr^{-1}$ for 2000 using NO_2 columns observed by the Global Ozone Monitoring Experiment (GOME) instrument, a factor of two higher than the Yienger and Levy (1995) a priori inventory used in their CTM. In another study by Bertram et al. (2005), short intense NO_x pulses following fertiliser application and precipitation were observed using satellite NO_2 observations from the SCIAMACHY (SCanning Imaging Absorption spectroMeter for Atmospheric CHartographY) instrument. Regional top-down soil NO_x estimates have been reported using the GOME instrument for eastern China (Wang et al., 2007), and using OMI for Mexico (Boersma et al., 2008) and eastern China (Zhao and Wang, 2009). These studies found substantial increases in soil NO_x emissions of 140 % to 350 % compared to the bottom-up inventories of 6.2 $Tg\,N\,yr^{-1}$ globally from Wang et al. (1998). Recently, Lin (2012) derived 25 % lower soil NO_x emissions than the Hudman et al. (2012) a priori for East China using OMI NO_2 columns. Nevertheless, his estimate is also higher than the 5–6 $Tg\,N\,yr^{-1}$ calculated with the Yienger and Levy (1995) or Wang et al. (1998) model. Although these regional satellite studies are all indicating stronger than 5–6 $Tg\,N\,yr^{-1}$ soil NO_x emissions, the global total of soil NO_x emissions remains uncertain.

Here we present top-down constraints on global soil NO_x emissions based on OMI NO_2 columns. We provide, for the first time, a specific top-down soil NO_x emissions inventory based on OMI constraints on all major continents. NO_2 concentrations simulated with these top-down emissions are subsequently validated against surface NO_2 measurements in Africa, the USA and Europe.

2 Model and observations

2.1 GEOS-Chem

We used the GEOS-Chem chemistry transport model (v9-02l, http://geos-chem.org) to simulate global tropospheric NO_2 columns for 2005. GEOS-Chem was operated at $2^\circ \times 2.5^\circ$ resolution

with 47 vertical layers, and a transport and chemistry time step of 15 and 30 min, respectively. Model simulations were driven by GEOS-5 assimilated meteorological observations from the NASA Global Modeling and Assimilation Office (GMAO). The vertical extent of the model is 80 km, and the lowest model layer has a depth of about 120 m. The detailed ozone-NO_x-hydrocarbon-aerosol chemistry of GEOS-Chem was recently described by Mao et al. (2010) and Lin et al. (2012). The current chemical mechanism in GEOS-Chem includes the most recent JPL/IUPAC recommendations as implemented by Mao et al. (2013). Recent updates to the GEOS-Chem model include 3 hourly GFED v3 biomass emissions (van der Werf et al., 2010; Mu et al., 2011), a look-up table to account for the non-linear NO_x chemistry in ship plumes (Vinken et al., 2011), constraints on lightning NO_x emissions with LIS/OTD satellite data (Murray et al., 2012), and implementation of a new soil NO_x module (Hudman et al., 2012). We performed a spin-up of one year (2004) and output simulated tropospheric NO_2 columns corresponding to the OMI overpass time (between 13:00 and 15:00 LT) for 2005. We selected simulated columns according to our filtering scheme of Sect. 3.1, and corresponding to days with valid satellite observations (see next section). The averaging kernel provided along with the OMI retrieval has been applied on the GEOS-Chem NO_2 columns in this study to account for the vertical sensitivity of the satellite instrument.

Global anthropogenic emissions are from the EDGAR 3.2FT2000 inventory (Olivier and Berdowski, 2001) for 2000 (van Donkelaar et al., 2008). This global inventory is replaced with regional inventories over Europe (EMEP), the United States (NEI2005), Canada (CAC), Mexico (BRAVO), and East Asia (Streets et al., 2006). Other NO_x emission sources in GEOS-Chem include lightning (Sauvage et al., 2007; Murray et al., 2012), biofuel (Yevich and Logan, 2003) and aircraft (Baughcum et al., 1996).

Soil NO_x emissions are from the parameterisation described in Hudman et al. (2012). This parameterisation does not provide a canopy reduction factor (CRF), which accounts for the fraction of NO_x that is deposited within the canopy before it reaches the atmosphere. Here we document the development of an update to the CRF of Jacob and Bakwin (1991), implemented in GEOS-Chem by Wang et al. (1998). We integrated the land cover system introduced by Steinkamp and Lawrence (2011) (based on MODIS satellite data (Friedl et al., 2002) and

Köppen main climate classes (Kottek et al., 2006)) with the Wang et al. (1998) CRF, and updated the CRF calculation to use the MODIS leaf area index (Yang et al., 2006). This CRF is based on physical considerations, and depends on canopy surface resistance for deposition of NO_x, above-canopy wind speed, and leaf area index. The dependence on wind speed enhances canopy uptake in situations of low wind speed, and the leaf area index dependence accounts for enhanced uptake in grid cells with large leaf surface areas. Figure 2 shows that the smallest CRFs are calculated over tropical forests in South America and Africa (as low as 0.15), reflecting strong uptake of soil emissions by deep canopies in the tropics (a CRF of 1 corresponds to zero canopy uptake). Only modest reduction factors of 0.95 are calculated over semi-arid savannahs like the Sahel, and the global average CRF is 0.87. The above-canopy total of soil NO_x emissions in GEOS-Chem amounts to 9.6 $Tg\,N$ for 2005 (Fig. 3a), and is higher than the Hudman et al. (2012) total (of 9.0 $Tg\,N$ for 2006) mainly because their study reports an above-canopy total using a monthly averaged CRF from Wang et al. (1998).

Table 1 lists NO_x emission totals for 2005 used in this study. 65 % of global NO_x emissions in 2005 are from anthropogenic sources (33.4 $Tg\,N\,yr^{-1}$; including aircraft, biofuel, and fertiliser use). However, in Northern Hemisphere summer months natural emissions (biomass burning, lightning and soil) are a substantial source, accounting for 47 % of global NO_x emissions in May–September 2005.

2.2 OMI measurements

The Ozone Monitoring Instrument (OMI) is a nadir-viewing UV/visible imaging spectrograph aboard the Aura satellite (Levelt et al., 2006). Aura crosses the Equator at 13:40 LT in a polar orbit, and OMI measurements are available since December 2004. The spatial resolution of OMI measurements is up to $13\,km \times 24\,km$ for nadir pixels and OMI achieves global coverage every day. Here we use tropospheric NO_2 vertical column densities from the Dutch OMI tropospheric NO_2 (DOMINO) v2.0 product (Boersma et al., 2011) (available from the Tropospheric Emissions Monitoring Internet Service (TEMIS); http://www.temis.nl). Retrieval errors over remote unpolluted areas are dominated by uncertainties in spectral fitting ($0.7 \times 10^{15}\,molecules\,cm^{-2}$) (Boersma et al., 2007). Other errors resulting from incorrect as-

sumptions about aerosols, surface albedo, clouds or the NO_2 vertical profile dominate errors over polluted regions (Boersma et al., 2004). The total error budget for DOMINO v2.0 is estimated to be 1.0×10^{15} molecules $cm^{-2} + 25\,\%$ for individual retrievals (Boersma et al., 2011). DOMINO v2.0 NO_2 retrievals have been validated with in-situ observations (e.g. Irie et al., 2012) and have recently been used in several studies to constrain NO_x emissions (e.g. Lu and Streets, 2012; Stavrakou et al., 2013; Vinken et al., 2014; McLinden et al., 2014).

To reduce retrieval errors we exclude clouded scenes, and snow or ice covered pixels (scenes with a cloud radiance fraction above 0.5, or surface albedo above 0.2). Effective cloud fractions are from the OMI O_2-O_2 retrieval (OMCLDO2) (Acarreta et al., 2004; Sneep et al., 2008), and OMI surface albedos are taken from Kleipool et al. (2008). Spatial smearing due to viewing geometry is reduced by removing the outer 2 (large) pixels on each side of the swath. We regrid OMI pixels to the GEOS-Chem horizontal grid ($2^\circ \times 2.5^\circ$), requiring that more than 75 % of a grid cell is covered by OMI observations~~, and that there are more than 3 observations per monthly average in each grid cell.~~. For a grid cell to be included we require 75% of a grid cell to be covered by valid OMI observations, so we typically have at least 200 observations per grid cell per month.

2.3 Surface measurements

2.3.1 IDAF

We used monthly surface NO_2 measurements from the International Global Atmospheric Chemistry (IGAC)/Deposition of Biochemically Important Trace Species (DEBITS)/Africa (IDAF) network in Africa (http://idaf.sedoo.fr). These measurements are obtained with passive samplers (Galy-Lacaux et al., 2001), have a detection limit of 0.2 ppbv and the reproducibility is 10 %. A detailed description of the IDAF monitoring stations, the sampling procedure and chemical analysis of samples, as well as the validation method according to international standards, can be found in Adon et al. (2010). NO_x measurements from IDAF sites were used by Jaeglé et al. (2004) to demonstrate the pulsing effect of soil NO_x emissions in the Sahel region. In this study we compare IDAF measurements (taken on a monthly basis) to GEOS-Chem sim-

ulated surface NO_2 concentrations for three IDAF sites (Banizoumbou in Niger, Agoufou and Katibougou in Mali; see Fig. S1 for locations). These three IDAF sites are located in remote rural areas in the Sahel (see Fig. S1 for 2005–2008 averaged OMI NO_2 columns over this region), and are representative of a dry savanna ecosystem (Adon et al., 2010).

2.3.2 EMEP

Daily surface measurements of NO_2 were used from 3 monitoring sites of the European Monitoring and Evaluation Programme (EMEP; available at http://www.emep.int) (Tørseth et al., 2012). All selected sites are located in Poland in a region dominated by soil NO_x emissions and small contributions from other NO_x sources (see Fig. S1 for locations). Two sites (Jarczew and Leba) use an iodide absorption method to measure NO_2 concentrations, and a third site (Diabla Gora) uses a filter-pack method (EMEP/CCC, 2001). The detection limit of the iodide absorption method is 0.3 ppbv, and 0.03 ppbv for the filter-pack method. Relative standard deviations (RSD) are reported to be better than 6 % (Aas, 2007). EMEP measurements are intended to reflect regional background conditions, relatively unaffected by substantial nearby (non-soil) NO_x emissions (see OMI NO_2 columns over this region in Fig. S1).

2.3.3 EPA

We used hourly NO_2 measurements from 11 sites in the Midwestern USA from the Environmental Protection Agency (EPA) network (see Fig. S1 for locations). These sites use chemiluminescence analysers, which measure NO_2 concentrations indirectly as the difference between nitrogen oxides (NO_x) and nitric oxide (NO) (US Environmental Protection Agency, 1995). NO is measured by the chemiluminescence following its reaction with O_3. NO_x is measured in the same way after first passing the sample through a molybdenum converter that converts NO_2 to NO. The NO_2 detection limit of chemiluminescence monitors is reported to be below 0.1 ppbv (Parrish and Fehsenfeld, 2000). Although commonly applied, this method can lead to an overestimation of NO_x (and NO_2) concentrations, as other reactive nitrogen species (peroxyacetyl nitrate, nitric acid, and organic nitrates) can also be converted to NO (US Envi-

ronmental Protection Agency, 1995). Steinbacher et al. (2007) showed that these biases can be up to +50 % for a rural area downwind of pollution sources in Switzerland. We selected these 11 sites as they are classified as rural sites, and are representative of background concentrations (i.e. unaffected by strong local anthropogenic emissions, see Fig. S1).

3 Methods

3.1 Filtering

Contributions of soil NO_x emissions to the total tropospheric NO_2 column can often be overshadowed by strong signals from other sources (e.g. anthropogenic, biomass burning or lightning). We introduce a filtering scheme to optimise detection of soil NO_x signals in OMI NO_2 columns. In this scheme, we select modelled and observed NO_2 columns with a: (1) fraction of soil NO_x emissions to the modelled tropospheric NO_2 column larger than 30 %, (2) fraction of biomass burning emissions less than 30 %, (3) fraction of lightning emissions less than 50 %, and (4) absolute contribution of soil emissions to OMI NO_2 column larger than 0.2×10^{15} molec cm^{-2} (modelled fraction of soil emissions multiplied with OMI NO_2 column). We include an absolute (OMI) soil contribution filter as smaller signals ($< 0.2 \times 10^{15}$ molec cm^{-2}) are most likely undetectable in OMI NO_2 columns. By explicitly calculating the fraction of a particular emissions source to the NO_2 column, our filter reduces the possibility of biases that are correlated with soil NO_x emissions.

We found that determining the fraction of the modelled tropospheric NO_2 column ~~of~~ due to a particular source by simply turning off that source is inadequate because of considerable non-linearities in NO_x-chemistry. In this study we apply a new method, in which we first simulate NO_2 columns following a 1 % increase in overall emissions. Next, we simulate NO_2 columns following a 1 % increase in a specific emission source (i.e. soil, lightning, or biomass burning). The fraction of a specific emission source i is then calculated by

$$\lambda_i = \frac{N_{\mathrm{GC},i,101\,\%} - N_{\mathrm{GC},100\,\%}}{N_{\mathrm{GC,all},101\,\%} - N_{\mathrm{GC},100\,\%}} \quad (1)$$

with λ_i the fraction of the modelled tropospheric NO_2 column of emission source i in a grid cell, $N_{GC,i,101\,\%}$ ~~the response of the modelled NO_2 column to increasing emission source i with 1 %~~ the modelled NO_2 column obtained by increasing emission source i by 1 %, $N_{GC,100\,\%}$ the modelled NO_2 column with regular (100 %) emissions, and $N_{GC,all,101\,\%}$ the NO_2 column ~~response to~~ obtained by increasing all emissions in a grid cell by 1 %. This approach accounts for non-linearities in NO_x chemistry, since the non-linear relationship between an emission increase and column response is explicitly calculated. Figure 3 shows soil NO_x emissions in GEOS-Chem (Fig. 3a), and the fraction (λ_{soil}) of the simulated NO_2 column originating from soil NO_x emissions (Fig. 3b). The fraction of the modelled tropospheric NO_2 column of soil NO_x (λ_{soil}) shows clear hotspots (of up to 75 %) in areas with strong soil NO_x emissions. Figure 3c shows that these areas also show high absolute contributions (of up to 2×10^{15} molec cm^{-2}) of soil emissions to the OMI NO_2 column. We identified 11 regions where soil NO_x emissions dominate the tropospheric NO_2 column, with $\overline{\lambda_{soil}} = 0.45$ for June (Northern Hemisphere) and December (Southern Hemisphere) 2005, by applying our filter scheme on monthly averaged modelled and observed NO_2 columns (regions indicated in Fig. 3b and c). For the Spain-France and Eastern Europe regions we adapted our filter slightly (requiring $\lambda_{soil} > 0.2$), as otherwise the number of samples in these regions would be too low to do a meaningful statistical comparison. Although Fig. 3c shows that the absolute contribution of soil NO_x to the OMI NO_2 column in South-East Asia is high (up to 2×10^{15} molec cm^{-2}), the fraction of soil NO_x contribution to this column is low (only 15–25 %; Fig. 3b) as anthropogenic emissions dominate the (high) NO_2 columns in this area.

We test our filtering scheme by calculating the correlation between GEOS-Chem NO_2 columns and soil NO_x emissions for all 11 regions in 2005. Figure 4 shows the relationship between NO_2 columns and local soil NO_x emissions for 3 months with highest soil NO_x emissions in the Sahel, India and Australia. Reduced Major Axis (RMA) fit lines and regression statistics are shown (for all months and regions see Table S1). The strong correlations ($R^2 > 0.43$ for all months shown in Fig. 4) indicate that spatial patterns in modelled NO_2 columns indeed reflect the underlying soil NO_x emissions. This allows us to use OMI observed NO_2 columns to constrain soil NO_x emissions in the identified regions. We require that the spa-

tial correlation (R^2) between soil NO_x emissions and modelled NO_2 columns is better than 0.2 in order to prevent misattribution of NO_2 to soil NO_x emissions. Slopes of the RMA regression fits represent the relationship between NO_x emissions and NO_2 columns in different chemical regimes. The variation in this relationship between regions (and chemical regimes) is a clear example of the non-linearity of NO_x chemistry and the dependence on OH availability. For example, slopes are higher (~ 0.3–0.5) for winter months (e.g. India or Sahel in Table S1), indicating that columns respond strongly to emissions changes in these months. Slopes are small (< 0.1) for relatively clean areas (e.g. Australia), indicating that an increase in emissions leads only to small column changes. This is the result of the non-linear feedback of NO_x on OH concentrations, reducing the NO_x lifetime. When constraining NO_x emissions using modelled and observed NO_2 columns ~~such non-linearities~~ the variability of NO_2 column lifetime needs to be taken into account.

3.2 Constraining a priori soil NO_x emissions

We calculate top-down soil NO_x emissions ($E_{\text{top down}}$) for the 11 regions using the mass-balance approach (e.g. Martin et al., 2003; Lamsal et al., 2011). First, we fit an RMA regression to all monthly averaged OMI and GEOS-Chem NO_2 column pairs within an area. We then use the slope (κ) of this RMA regression to scale the a priori soil NO_x emissions ($E_{\text{a priori}}$) in GEOS-Chem. Using the slope (instead of a local ratio of total modelled and observed NO_2 columns) accounts for any bias that may be present in observed and modelled columns (through the offset in the regression). We calculate the (regional average) OMI top-down soil NO_x inventory by:

$$E_{\text{top down}} = E_{\text{a priori}} + (\kappa - 1) \cdot \beta' \cdot E_{\text{a priori}} \quad (2)$$

with β' the factor taking into account the non-linearities in NO_x–O_3 chemistry (Lamsal et al., 2011). These non-linearities arise from the feedback of NO_x concentrations on its own oxidation losses (i.e. lifetime, via OH availability). The β' factor represents the (modelled) local sensitivity of NO_2 column changes to NO_x emission perturbations, and differs from the β of Lamsal et al. (2011) as we apply the DOMINO averaging kernel on simulated NO_2 columns

in our β' calculations. In this study we calculated β' by perturbing surface emissions in our selected regions by 10 %: ~~(this percentage was calculated using the averaged κ over all regions)~~. ~~We expect our β values to be somewhat higher than in the Lamsal et al. (2011) approach due to boundary effects (there is no enhanced NO_2 inflow from areas outside the boundaries of our regions), and because most of the 11 areas are characterised as low NO_x regimes, which are known to be very sensitive to OH-feedback following NO_x increases. We calculated β' by:~~

$$\beta' = \frac{\Delta E/E}{\Delta N'_{GC}/N'_{GC}} \tag{3}$$

with E the surface NO_x emissions, N'_{GC} the simulated tropospheric NO_2 column (with the DOMINO averaging kernel applied), ΔE the increase in surface NO_x emissions, and $\Delta N'_{GC}$ the subsequent change in simulated tropospheric NO_2 columns (with the DOMINO averaging kernel applied). Table 2 shows β' factors calculated using monthly averaged perturbed NO_2 columns over the 11 regions (sampled following our filtering scheme of Sect. 3.1). To allow for a comparison with Lamsal et al. (2011), unfiltered β values (calculated without application of the averaging kernel) are provided in the Supplementary Material. Our β' values ($\overline{\beta'} = 2.45$) are ~~high, but compare well to~~ higher than β values found by Lamsal et al. (2011) (see their Fig. S1) ~~for areas with low NO_x concentrations~~. We find that differences versus Lamsal et al. (2011) are mostly driven by the application of the averaging kernel on GEOS-Chem simulated NO_2 columns in our study, which increases β' by about 30% compared to β (see Supplementary Material). Other differences versus Lamsal et al. (2011) arise from our focus on low NO_x environments which are sensitive to OH-feedbacks, from our focus on selected months when conditions are favourable for OH production (see seasonal cycle of β' and β in Tables 2, S4, and S5), and to a lesser extent from boundary effects (due to the absence of enhanced NO_x inflow from sources outside the region). ~~In our study, β factors are higher because the selected months are predominantly in summer, when conditions are favourable for OH production. This effect can be observed in the seasonal cycle of β (Tables 2 and S4), which shows highest β values in summer months.~~ We ~~furthermore~~ also observe that for areas with high ambient NO_x concentrations (e.g. India or west-USA), β' values are indeed lower ($\sim$ 1.5–2.2) than over pristine

remote areas like Australia ($\beta' \sim 2.7$–3.4). These different β' values illustrate different chemical regimes, and the need to account for non-linearities in NO_x-chemistry.

4 Results

4.1 Comparison modelled and satellite observed NO_2 columns

We compare OMI and GEOS-Chem NO_2 columns for the 11 identified regions in 2005. As an example, Fig. 5a shows the relationship between OMI and GEOS-Chem NO_2 columns for the Sahel in May. There is a high degree of correlation ($R^2 = 0.71$) between observed and simulated spatial patterns in NO_2 columns, and the Figure shows that OMI generally observes higher NO_2 columns than simulated by GEOS-Chem with a priori soil NO_x emissions (slope $\kappa = 1.48$ using an RMA regression). Correlations between observed and simulated NO_2 columns are strong ($R^2 > 0.5$) in all months over the Sahel, with κ generally above 1 suggesting that the prior soil NO_x emissions are systematically too low (Table S2). For other regions, fit statistics generally also show strong correlations, especially for summer months with highest emissions. For some regions, we found moderate correlations between observed and simulated NO_2 columns patterns (e.g. $R^2 < 0.3$ for India in March). Such correlation coefficients are probably indicative of errors in non-soil NO_x emissions, including spatial misplacement of such emissions. We exclude months with moderate correlations ($R^2 < 0.$[illegible]) in our top-down constraints, because for these months and regions OMI NO_2 observations cannot be interpreted to provide an unambiguous attribution to soil NO_x emissions. We found 51 months and regions with sufficient spatial correlation between GEOS-Chem soil NO_x emissions and NO_2 columns, and between GEOS-Chem and OMI NO_2 columns, to anticipate a meaningful constraint by OMI on soil NO_x emissions. Figure 5b summarises the comparisons for all months and regions (in red for the Northern Hemisphere, in black for the Southern Hemisphere). This Figure shows that slopes are generally above unity, and there are no indications that slopes are systematically different for regions situated in the Northern vs. Southern Hemisphere.

4.2 OMI top-down soil NO_x emissions

We continue and calculate constraints ($(\kappa - 1) \cdot \beta'$) for the 51 identified months and regions. We apply these constraints in Eq. (2) to calculate new OMI top-down soil NO_x emissions. Our top-down mass-balance approach provides constraints for 13 % of global soil NO_x emissions over the 11 identified regions for 51 months (regional annual a priori emission totals are given in Table 1). Figure 6a shows that the top-down soil NO_x inventory results in a global total of 10.0 $Tg\,N\,yr^{-1}$. Substantial regional differences (e.g. +60 % for Eastern Europe and South Kazakhstan; and −40 % for Midwestern USA; see Fig. 6c and d) exist compared to the GEOS-Chem a priori (Fig. 6b), and overall the top-down inventory is 4 % higher than the a priori. Figure 6c shows that, except for the Midwestern USA, annual emissions increase for all regions in the OMI top-down inventory. The seasonal variation in a priori and top-down soil NO_x emissions for the Sahel, the Midwestern USA, Australia, and Eastern Europe is given in Fig. 7. For the Sahel (Fig. 7a), OMI on average indicates 20 % higher emissions and suggests a stronger seasonal cycle than the a priori inventory. The OMI inferred Sahel estimate is 0.52 $Tg\,N\,yr^{-1}$, comparable to the value of 0.56 $Tg\,N\,yr^{-1}$ found by extrapolating the Delon et al. (2010) estimate ($0.35 \pm 0.11\,Tg\,N\,yr^{-1}$ for 2006 based on upscaling 3 surface observations) to our Sahel domain size. For the Midwestern USA (Fig. 7b), our new inventory is substantially lower (−40 %), and indicates zero soil NO_x emissions for July. It is unlikely that soil emissions are zero in this month, pointing at other NO_x sources in this region in need of reduction, or errors in NO_x chemistry. Figure 7c shows that the OMI top-down inventory also suggests a stronger seasonal cycle for Australia, and emissions increase by 90 % for this region relative to the bottom-up inventory. For Eastern Europe, emissions increase by 60 %, and there seems to be a temporal shift in soil NO_x emissions towards late summer. Our analysis shows that in general OMI suggests higher soil NO_x emissions for months with already enhanced emissions (i.e. summer months), indicating directions for future improvements to state-of-science parameterisations. The average increase of emissions in all 11 regions is +35 % (from 1.2 to 1.6 $Tg\,N\,yr^{-1}$). Figure 8 shows that extrapolating this 35 % increase in emissions to all regions with soil NO_x emissions results in 12.9 $Tg\,N\,yr^{-1}$.

We proceed and simulate NO_2 columns using our new OMI top-down soil NO_x emissions. The relationship between these new GEOS-Chem and OMI NO_2 columns for the Sahel in May is given in Fig. 5c. This Figure shows that GEOS-Chem NO_2 columns simulated using the new top-down inventory agree better with OMI NO_2 columns than the a priori (slope κ closer to 1). Figure 5d shows the summary of the comparison between GEOS-Chem NO_2 columns based on the top-down soil NO_x emissions and OMI NO_2 observations for all regions and months. In general, all slopes improve (closer to unity), and correlation coefficients decrease slightly (on average 7 % lower). For South-Kazakhstan in May, we found no spatial correlation between OMI and GEOS-Chem NO_2 columns (orange dot in Fig. 5d). For this case, ~~with just sufficient correlations~~ the correlation between soil NO_x emissions and modelled NO_2 columns, as well as between OMI and GEOS-Chem was sufficient (see Tables S1 and S2), and the fitted RMA slope suggests that a priori emissions are too low ($\kappa = 2.6$). Although the absolute values of the GEOS-Chem NO_2 columns based on the top-down emissions better represent the range observed in the OMI NO_2 columns, there is no spatial correlation between GEOS-Chem and OMI NO_2 columns. This is an indication of an error in the spatial distribution of the soil NO_x emissions, and a local scaling approach is probably required here.

We acknowledge that our top-down emissions do not lead to improved spatial agreement between GEOS-Chem simulations and OMI columns, but merely provide an improved estimate of the total mass of N emitted from soils within an area. Furthermore, a perfect match between OMI and GEOS-Chem NO_2 columns is not expected, as we only apply our constraints to soil emissions (which constitute a fraction of the total emissions within a grid cell). The much improved quantitative agreement between OMI and GEOS-Chem shows that the relatively high β' values describe the non-linear response of the NO_2 column to changes in NO_x emissions to a reasonable degree, and allow us to constrain soil NO_x emissions in one iteration.

4.3 Validation against surface measurements

We used surface measurements of NO_2 to evaluate GEOS-Chem simulations based on the OMI top-down soil NO_x inventory. Monthly averaged simulated and in-situ observed surface NO_2 concentrations are compared for the Sahel (IDAF measurements), Midwestern USA (EPA mea-

surements), and Eastern Europe (EMEP measurements; see Fig. S1 for locations of measurement stations). These locations were selected as these areas are dominated by soil NO_x emissions (see Fig. 3b and c), and are located away from other strong (anthropogenic) NO_x sources (see Fig. S1 for 2005–2008 averaged OMI NO_2 columns over these regions). We averaged simulated NO_2 concentrations in grid cells containing in-situ monitors for months with OMI constraints. We compared these simulations to the spatial average of all monitors in a region (if available). Figure 9a shows the agreement between surface NO_2 concentrations simulated with the a priori soil NO_x emissions and the in situ measurements for the three regions. We observe a weak correlation ($R^2 = 0.2$) and a fitted RMA regression slope of 0.7, which confirms that GEOS-Chem underestimates soil NO_x emissions. Application of the OMI soil NO_x emissions leads to an improved (moderate) correlation and slope ($R^2 = 0.31$, with a slope of 0.83; and Root-Mean-Squared-Error (RMSE) decreases by 5 %) (Fig. 9b), demonstrating the value of the improved satellite-based soil NO_x emissions against independent measurements. The error bars in Fig. 9 indicate the typical uncertainties in modelled and observed concentrations, and take into account reproducibility (~ 10 % for IDAF), interference (~ 20 % for EPA), and representativeness errors due to averaging over multiple stations. We cautiously estimate the overall error in our surface observations to be around 0.5 ppbv, with an important contribution from representativeness errors. The error in the simulated surface NO_2 concentrations, caused by both errors in the soil NO_x emission inventory and other model errors (see next section), is estimated to be around 0.4 ppbv.

The comparison of monthly averaged modelled and observed NO_2 concentrations for the Sahel is shown in Fig. 9c, and indicates that simulations with our new inventory better capture the seasonal peak of NO_2 concentrations in April–August following enhanced soil NO_x emissions. However, GEOS-Chem does not simulate the second peak of measured NO_2 concentrations in September–November. This peak corresponds with the beginning of the dry season and is the result of biomass burning in the region (Jaeglé et al., 2004; Adon et al., 2010). For the Sahel in 2005, the correlation (R^2) between modelled and observed NO_2 concentrations improves (from 0.21 to 0.39), and the RMSE decreases by 8 % when using the new OMI top-down inventory in our simulations.

We note that several factors complicate the comparison between surface measurements and simulated concentrations by a (global) CTM. First, measurements by one in-situ monitor are unlikely to be horizontally representative of concentrations simulated for an entire ($2^\circ \times 2.5^\circ$) model grid cell. Furthermore, the in-situ monitors sample air at 2 m height, and the lowest GEOS-Chem grid cell is centred at 58 m. Also, observations can be considerably influenced by systematic measurement errors (e.g. interference in the chemiluminescence analysers). Finally, errors in simulated concentrations can arise from incorrect vertical mixing, non-soil NO_x emissions, or N-input from manure. Nevertheless, our results are encouraging, and indicate improved agreement between measured and simulated NO_2 concentrations when using the OMI top-down soil NO_x emission inventory.

4.4 Errors in top-down inventory and surface concentrations

Uncertainties in our OMI top-down soil NO_x inventory originate from a combination of errors in the GEOS-Chem model, OMI satellite observations, and our mass-balance approach. Systematic model errors arise from incorrect assumptions about NO_x chemistry, emissions or vertical mixing. This study attempts to reduce one such systematic error, i.e. soil NO_x emissions. We estimate the remaining model error to be around 25 % (see Martin et al., 2003; Lin et al., 2012; Lin, 2012; Stavrakou et al., 2013, for a discussion on these model errors). Satellite observations from OMI have a systematic and random error part, and the total error for a single NO_2 column is 1.0×10^{15} molecules cm^{-2} + 25 % (Boersma et al., 2011). Random errors in the OMI observations are reduced by monthly averaging NO_2 columns, but systematic biases might still persist. Our inversion approach is based on a regression that compares observed and modelled spatial NO_2 patterns that are directly associated with soil NO_x emission patterns. Such an approach will be robust to absolute biases in either OMI or GEOS-Chem columns, as long as these biases are unrelated to the soil NO_x emissions, but can still be sensitive to relative biases in either model or observations. The remaining error in the OMI observations is estimated to be around 20 % (see Irie et al., 2012; McLinden et al., 2014, for a discussion). Errors in our constraints arise from uncertainties in β' values and fitted RMA slopes (κ). To first order our method is independent of the a priori inventory, and mainly sensitive to mis-

placement of emissions in the a priori inventory. We minimise this error due to misplacement of emissions by requiring a strong ($R^2 > 0.35$) correlation between OMI and GEOS-Chem NO_2 columns. Errors in the calculated β' values have systematic (as a result of model errors) and random components. Lamsal et al. (2011) showed that variations in β are small ($< 5\,\%$) when varying the emission perturbation, and we estimate the overall error in β' at 25 % (in line with β-uncertainties quoted by Castellanos et al., 2014). The statistical error in the fitted RMA slope is 5–13 % for the Sahel, and we cautiously estimate the overall error in the fitted RMA slopes for all regions at 15 %. Using standard error propagation for the relevant error components of Eq. (2), and assuming the errors to be largely uncorrelated, we calculated that typical errors on our top-down soil NO_x inventory are around 30 %. We found largest errors for small κ and large β' values. This indicates that space-based constraints are generally most difficult for strongly non-linear NO_x regimes (with high β': strong changes in emissions result in small column changes only), and small signals observed by OMI (indicated by low kappa), as the (relative) retrieval error is highest under such situations (with contributions from noise and AMF errors).

5 Conclusions

We present a method to provide top-down constraints on soil NO_x emissions using OMI tropospheric NO_2 columns and simulations from the GEOS-Chem global CTM. We develop a filtering scheme to select regions and periods wherein OMI tropospheric NO_2 columns are dominated by soil NO_x emissions, with minimal influence of anthropogenic, lightning, and biomass burning sources. Focusing on the year 2005, we find 11 regions, distributed over all the major continents, where soil NO_x emissions are driving tropospheric NO_2 column patterns in the warm season, as demonstrated by the generally strong spatial correlation between soil NO_x emission and tropospheric NO_2 column patterns in both GEOS-Chem and OMI fields. These regions are generally away from major anthropogenic and biomass burning NO_x source areas, and either dominated by agricultural (e.g. the Midwestern USA) or biogenic (e.g. the Sahel) soil NO_x emissions.

The strong correlation between tropospheric NO_2 column patterns and soil NO_x emissions allows us to attribute enhancements in OMI NO_2 observations to soil NO_x emissions. Using a mass-balance approach for each of the 11 soil NO_x-dominated regions, we calculate top-down constraints on soil NO_x emissions based on OMI and GEOS-Chem NO_2 columns. Our approach takes full account of non-linearities in NO_x chemistry. The sensitivity of simulated NO_2 columns to changing NO_x emissions (the so-called beta-factor) proves to be strongly non-linear over regions dominated by soil NO_x emissions. Beta-values are generally about 2.5, illustrating the strong negative feedback of NO_x emissions onto the daytime NO_2 abundances (through loss against enhanced OH) in warm months over the 11 regions. In contrast to anthropogenic NO_x source regions where NO_2 responds rather linearly to changes in NO_x emissions, our simulations highlight the relevance of taking non-linearities in account over low-NO_x regimes.

For most regions and months, OMI observes higher NO_2 columns than simulated by GEOS-Chem based on a recent a priori soil NO_x emission inventory proposed by Hudman et al. (2012), incorporating emission factors from Steinkamp and Lawrence (2011). From our mass-balance approach, and accounting for non-linear NO_x chemistry, we infer increases of about 50 % in monthly regional soil NO_x emissions. These increases translate into a global OMI top-down soil NO_x inventory total of 10.0 Tg N for 2005 (when only constraining the 11 regions), and 12.9 Tg N (when extrapolating the constraints globally), 4–35 % higher than the GEOS-Chem a priori (9.6 Tg N yr^{-1}). We find substantial regional differences (ranging from -40 % to $+90$ %), e.g. annual emissions in the Sahel are 20 % higher and indicate a stronger seasonal cycle.

To our knowledge, this study provides, for the first time, specific constraints on soil NO_x emissions on all 5 major continents using OMI NO_2 columns. Our results rule out the low ~~high~~ end of reported soil NO_x emission estimates, and suggest that global emissions are most likely around ~~10–13~~12.9$\pm$3.9 Tg N yr^{-1} (by constraining 13% of all global soil NO_x emissions). The OMI top-down inventory indicates that emissions need to be substantially increased in most regions, implying upward corrections to emissions factors currently used in the GEOS-Chem soil NO_x parameterisation. We evaluate NO_2 concentrations simulated with our new OMI top-down inventory against surface NO_2 measurements from monitoring stations in Africa (IDAF),

the USA (EPA), and Europe (EMEP). Although a comparison of measured and simulated surface NO_2 concentrations is complicated because of horizontal and vertical representativity, and by measurement errors, we find somewhat improved agreement when using the OMI top-down inventory. For the Sahel region, the seasonal peak of NO_2 concentrations in April–August is better captured by simulations with our new top-down soil NO_x inventory.

Our method can be applied in future studies using satellite NO_2 observations to reduce the range in soil NO_x emissions estimates. We find that OMI suggests a stronger seasonal cycle for the Sahel and Australia, and a shift in seasonality in Eastern Europe. Future work should focus on understanding these differences between top-down and a priori inventories, which can provide valuable information to improve current soil NO_x parameterisations. Furthermore, the parameterisation of fertiliser emissions could be improved upon (e.g. by improving manure-related processes in the model). Observations of other satellite instruments could also be used to study the diurnal variation of soil NO_x emissions, or to provide more constraints to further reduce current uncertainties in soil NO_x emissions.

The Supplement related to this article is available online at doi:10.5194/acpd-0-1-2014-supplement.

Acknowledgements. This research was funded by the Netherlands Organisation for Scientific Research, NWO Vidi grant 864.09.001. We thank Shailesh Kharol for helpful discussions in processing the EPA observations. The authors acknowledge data provided by participants of the EMEP and EPA measurement networks. We acknowledge the free use of tropospheric NO_2 column data from the OMI from www.temis.nl. We are also grateful to all the Principal Investigators (and field technicians) of the Sahelian IDAF sites, especially D. Laouali for Banizoumbou in Niger and B. Diop for Agoufou and Katibougou in Mali.

References

Aas, W.: Data quality 2005, quality assurance, and field comparisons, EMEP/CCC-Report 3/2007, Norwegian Institute for Air Research, Kjeller, 2007.

Acarreta, J. R., De Haan, J. F., and Stammes, P.: Cloud pressure retrieval using the O_2-O_2 absorption band at 477 nm, J. Geophys. Res.-Atmos., 109, D05204, doi:10.1029/2003JD003915, 2004.

Adon, M., Galy-Lacaux, C., Yoboué, V., Delon, C., Lacaux, J. P., Castera, P., Gardrat, E., Pienaar, J., Al Ourabi, H., Laouali, D., Diop, B., Sigha-Nkamdjou, L., Akpo, A., Tathy, J. P., Lavenu, F., and Mougin, E.: Long term measurements of sulfur dioxide, nitrogen dioxide, ammonia, nitric acid and ozone in Africa using passive samplers, Atmos. Chem. Phys., 10, 7467–7487, doi:10.5194/acp-10-7467-2010, 2010.

Baughcum, S. L., Tritz, T. G., Henderson, S. C., and Pickett, D. C.: Scheduled Civil Aircraft Emissions Inventories for 1992: Database Development and Analysis, NASA CR 4700, 1996.

Bertram, T. H., Heckel, A., Richter, A., Burrows, J. P., and Cohen, R. C.: Satellite measurements of daily variations in soil NO_x emissions, Geophys. Res. Lett., 32, L24812, doi:10.1029/2005GL024640, 2005.

Boersma, K. F., Eskes, H. J., and Brinksma, E. J.: Error analysis for tropospheric NO_2 retrieval from space, J. Geophys. Res., 109, D04311, doi:10.1029/2003JD003962, 2004.

Boersma, K. F., Eskes, H. J., Veefkind, J. P., Brinksma, E. J., van der A, R. J., Sneep, M., van den Oord, G. H. J., Levelt, P. F., Stammes, P., Gleason, J. F., and Bucsela, E. J.: Near-real time retrieval of tropospheric NO_2 from OMI, Atmos. Chem. Phys., 7, 2103–2118, doi:10.5194/acp-7-2103-2007, 2007.

Boersma, K. F., Jacob, D. J., Bucsela, E. J., Perring, A. E., Dirksen, R., van der A, R. J., Yantosca, R. M., Park, R. J., Wenig, M. O., Bertram, T. H., and Cohen, R. C.: Validation of OMI tropospheric NO_2 observations during INTEX-B and application to constrain emissions over the eastern United States and Mexico, Atmos. Environ., 42, 4480–4497, doi:10.1016/j.atmosenv.2008.02.004, 2008.

Boersma, K. F., Eskes, H. J., Dirksen, R. J., van der A, R. J., Veefkind, J. P., Stammes, P., Huijnen, V., Kleipool, Q. L., Sneep, M., Claas, J., Leitão, J., Richter, A., Zhou, Y., and Brunner, D.: An improved tropospheric NO_2 column retrieval algorithm for the Ozone Monitoring Instrument, Atmos. Meas. Tech., 4, 1905–1928, doi:10.5194/amt-4-1905-2011, 2011.

Bouwman, A. F., Boumans, L. J. M., and Batjes, N. H.: Emissions of N_2O and NO from fertilized fields: Summary of available measurement data, Global Biogeochem. Cy., 16, 6-1–6-13, doi:10.1029/2001GB001811, 2002.

Castellanos, P., Boersma, K. F., and van der Werf, G. R.: Satellite observations indicate substantial spatiotemporal variability in biomass burning NO_x emission factors for South America, Atmos. Chem. Phys., 14, 3929–3943, doi:10.5194/acp-14-3929-2014, 2014.

Conrad, R.: Soil microorganisms as controllers of atmospheric trace gases (H_2, CO, CH_4, OCS, N_2O, and NO), Microbiol. Rev., 60, 609–40, 1996.

Davidson, E.: Pulses of nitric oxide and nitrous oxide flux following wetting of dry soil: an assessment of probable sources and importance relative to annual fluxes, Ecol. Bull., 42, 149–155, 1992.

Davidson, E. and Kingerlee, W.: A global inventory of nitric oxide emissions from soils, Nutr. Cycl. Agroecosys., 48, 37–50, doi:10.1023/A:1009738715891, 1997.

Delon, C., Galy-Lacaux, C., Boone, A., Liousse, C., Serça, D., Adon, M., Diop, B., Akpo, A., Lavenu, F., Mougin, E., and Timouk, F.: Atmospheric nitrogen budget in Sahelian dry savannas, Atmos. Chem. Phys., 10, 2691–2708, doi:10.5194/acp-10-2691-2010, 2010.

Denman, K., Brasseur, G., Chidthaisong, A., Ciais, P., Cox, P., Dickinson, R., Hauglustaine, D., Heinze, C., Holland, E., Jacob, D., Lohmann, U., Ramachandran, S., da Silva Dias, P., Wofsy, S., and Zhang, X.: Couplings between changes in the climate system and biogeochemistry, in: Climate Change 2007: The Physical Science Basis, Contribution of Working Group I to the Fourth Assessment Report of the Intergovernmental Panel on Climate Change, Cambridge University Press, Cambridge, UK, New York, NY, USA, 499–587, 2007.

EMEP/CCC: Manual for Sampling and Chemical Analysis, Norwegian Institute for Air Research, Kjeller (Last rev. 2001), available at: http://www.nilu.no/projects/ccc/manual/index.html (last access: June 2014), 2001.

Firestone, M. and Davidson, E.: Exchange of Trace Gases Between Terrestrial Ecosystems and the Atmosphere, John Wiley, New York, 1989.

Friedl, M., McIver, D., Hodges, J., Zhang, X., Muchoney, D., Strahler, A., Woodcock, C., Gopal, S., Schneider, A., Cooper, A., Baccini, A., Gao, F., and Schaaf, C.: Global land cover mapping from MODIS: algorithms and early results, Remote Sens. Environ., 83, 287–302, doi:10.1016/S0034-4257(02)00078-0, 2002.

Galy-Lacaux, C., Carmichael, G. R., Song, C. H., Lacaux, J. P., Al Ourabi, H., and Modi, A. I.: Heterogeneous processes involving nitrogenous compounds and Saharan dust inferred from measurements and model calculations, J. Geophys. Res.-Atmos., 106, 12559–12578, doi:10.1029/2000JD900778, 2001.

Galbally, I. E. and Roy, C. R.: Loss of fixed nitrogen from soils by nitric oxide exhalation, Nature, 275, 734–735, doi:10.1038/275734a0, 1978.

Ganzeveld, L. N., Lelieveld, J., Dentener, F. J., Krol, M. C., Bouwman, A. J., and Roelofs, G.-J.: Global soil-biogenic NOx emissions and the role of canopy processes, J. Geophys. Res.-Atmos., 107, ACH 9-1–ACH 9-17, doi:10.1029/2001JD001289, 2002a.

Ganzeveld, L. N., Lelieveld, J., Dentener, F. J., Krol, M. C., and Roelofs, G.-J.: Atmosphere-biosphere trace gas exchanges simulated with a single-column model, J. Geophys. Res.-Atmos., 107, ACH 8-1–ACH 8-21, doi:10.1029/2001JD000684, 2002b.

Ghude, S. D., Kulkarni, S. H., Jena, C., Pfister, G. G., Beig, G., Fadnavis, S., and van der A, R. J.: Application of satellite observations for identifying regions of dominant sources of nitrogen oxides over the Indian Subcontinent, J. Geophys. Res.-Atmos., 118, 1075–1089, doi:10.1029/2012JD017811, 2013.

Hudman, R. C., Russell, A. R., Valin, L. C., and Cohen, R. C.: Interannual variability in soil nitric oxide emissions over the United States as viewed from space, Atmos. Chem. Phys., 10, 9943–9952, doi:10.5194/acp-10-9943-2010, 2010.

Hudman, R. C., Moore, N. E., Mebust, A. K., Martin, R. V., Russell, A. R., Valin, L. C., and Cohen, R. C.: Steps towards a mechanistic model of global soil nitric oxide emissions: implementation and space based-constraints, Atmos. Chem. Phys., 12, 7779–7795, doi:10.5194/acp-12-7779-2012, 2012.

IPCC: Climate Change 2007: Impacts, Adaptation and Vulnerability, Contribution of Working Group II to the Fourth Assessment Report of the Intergovernmental Panel on Climate Change, edited by: Parry, M. L., Canziani, O. F., Palutikof, J. P., van der Linden, P. J., and Hanson, C. E., Cambridge University Press, Cambridge, UK, 976 pp., 2007.

Irie, H., Boersma, K. F., Kanaya, Y., Takashima, H., Pan, X., and Wang, Z. F.: Quantitative bias estimates for tropospheric NO_2 columns retrieved from SCIAMACHY, OMI, and GOME-2 using a common standard for East Asia, Atmos. Meas. Tech., 5, 2403–2411, doi:10.5194/amt-5-2403-2012, 2012.

Jacob, D. J. and Bakwin, P. S.: Cycling of NO_x in tropical forest canopies and its implications for the global source of biogenic NO_x to the atmosphere, American Society of Microbiology, Washington DC, 1991.

Jaeglé, L., Martin, R. V., Chance, K., Steinberger, L., Kurosu, T. P., Jacob, D. J., Modi, A. I., Yoboué, V., Sigha-Nkamdjou, L., and Galy-Lacaux, C.: Satellite mapping of rain-induced nitric oxide emissions from soils, J. Geophys. Res.-Atmos., 109, D21310, doi:10.1029/2004JD004787, 2004.

Jaeglé, L., Steinberger, L., Martin, R. V., and Chance, K.: Global partitioning of NO_x sources using satellite observations: relative roles of fossil fuel combustion, biomass burning and soil emissions, Faraday Discuss., 130, 407–423, doi:10.1039/b502128f, 2005.

Kleipool, Q. L., Dobber, M. R., de Haan, J. F., and Levelt, P. F.: Earth surface reflectance climatology from 3 years of OMI data, J. Geophys. Res.-Atmos., 113, D18308, doi:10.1029/2008JD010290, 2008.

Kottek, M., Grieser, J., Beck, C., Rudolf, B., and Rubel, F.: World Map of the Köppen–Geiger climate classification updated, Meteorol. Z., 15, 259–263, doi:10.1127/0941-2948/2006/0130, 2006.

Lamsal, L. N., Martin, R. V., Padmanabhan, A., van Donkelaar, A., Zhang, Q., Sioris, C. E., Chance, K., Kurosu, T. P., and Newchurch, M. J.: Application of satellite observations for timely updates to global anthropogenic NO_x emission inventories, Geophys. Res. Lett., 38, L05810, doi:10.1029/2010GL046476, 2011.

Levelt, P. F., van den Oord en M. R. Dobber, G. H. J., Mälkki, A., Visser, H., de Vries, J., Stammes, P., Lundell, J. O. V., and Saari, H.: The Ozone Monitoring Instrument, IEEE T. Geosci. Remote, 44, 1093–1109, doi:10.1109/TGRS.2006.872333, 2006.

Lin, J.-T., McElroy, M. B., and Boersma, K. F.: Constraint of anthropogenic NO_x emissions in China from different sectors: a new methodology using multiple satellite retrievals, Atmos. Chem. Phys., 10, 63–78, doi:10.5194/acp-10-63-2010, 2010.

Lin, J.-T.: Satellite constraint for emissions of nitrogen oxides from anthropogenic, lightning and soil sources over East China on a high-resolution grid, Atmos. Chem. Phys., 12, 2881–2898, doi:10.5194/acp-12-2881-2012, 2012.

Lin, J.-T., Liu, Z., Zhang, Q., Liu, H., Mao, J., and Zhuang, G.: Modeling uncertainties for tropospheric nitrogen dioxide columns affecting satellite-based inverse modeling of nitrogen oxides emissions, Atmos. Chem. Phys., 12, 12255–12275, doi:10.5194/acp-12-12255-2012, 2012.

Lipschultz, F., Zafiriou, O. C., Wofsy, S. C., McElroy, M. B., Valois, F. W., and Watson, S. W.: Production of NO and N_2O by soil nitrifying bacteria, Nature, 294, 641–643, doi:10.1038/294641a0, 1981.

Lu, Z. and Streets, D. G.: Increase in NO_x emissions from Indian thermal power plants during 1996–2010: unit-based inventories and multisatellite observations, Environ. Sci. Technol., 46, 7463–7470, doi:10.1021/es300831w, 2012.

Ludwig, J., Meixner, F., Vogel, B., and Förstner, J.: Soil-air exchange of nitric oxide: an overview of processes, environmental factors, and modeling studies, Biogeochemistry, 52, 225–257, doi:10.1023/A:1006424330555, 2001.

Mao, J., Jacob, D. J., Evans, M. J., Olson, J. R., Ren, X., Brune, W. H., Clair, J. M. St., Crounse, J. D., Spencer, K. M., Beaver, M. R., Wennberg, P. O., Cubison, M. J., Jimenez, J. L., Fried, A., Weibring, P., Walega, J. G., Hall, S. R., Weinheimer, A. J., Cohen, R. C., Chen, G., Crawford, J. H., McNaughton, C., Clarke, A. D., Jaeglé, L., Fisher, J. A., Yantosca, R. M., Le Sager, P., and Carouge, C.:

Chemistry of hydrogen oxide radicals (HO_x) in the Arctic troposphere in spring, Atmos. Chem. Phys., 10, 5823–5838, doi:10.5194/acp-10-5823-2010, 2010.

Mao, J., Fan, S., Jacob, D. J., and Travis, K. R.: Radical loss in the atmosphere from Cu-Fe redox coupling in aerosols, Atmos. Chem. Phys., 13, 509–519, doi:doi:10.5194/acp-13-509-2013, 2013.

Martin, R. V., Jacob, D. J., Chance, K., Kurosu, T. P., Palmer, P. I., and Evans, M. J.: Global inventory of nitrogen oxide emissions constrained by space-based observations of NO_2 columns, J. Geophys. Res., 108, 4537, doi:10.1029/2003JD003453, 2003.

McLinden, C. A., Fioletov, V., Boersma, K. F., Kharol, S. K., Krotkov, N., Lamsal, L., Makar, P. A., Martin, R. V., Veefkind, J. P., and Yang, K.: Improved satellite retrievals of NO_2 and SO_2 over the Canadian oil sands and comparisons with surface measurements, Atmos. Chem. Phys., 14, 3637–3656, doi:10.5194/acp-14-3637-2014, 2014.

Miyazaki, K., Eskes, H. J., and Sudo, K.: Global NO_x emission estimates derived from an assimilation of OMI tropospheric NO_2 columns, Atmos. Chem. Phys., 12, 2263–2288, doi:10.5194/acp-12-2263-2012, 2012.

Mu, M., Randerson, J. T., van der Werf, G. R., Giglio, L., Kasibhatla, P., Morton, D., Collatz, G. J., DeFries, R. S., Hyer, E. J., Prins, E. M., Griffith, D. W. T., Wunch, D., Toon, G. C., Sherlock, V., and Wennberg, P. O.: Daily and 3-hourly variability in global fire emissions and consequences for atmospheric model predictions of carbon monoxide, J. Geophys. Res.-Atmos., 116, L05810, doi:10.1029/2011JD016245, 2011.

Müller, J.-F.: Geographical distribution and seasonal variation of surface emissions and deposition velocities of atmospheric trace gases, J. Geophys. Res.-Atmos., 97, 3787–3804, doi:10.1029/91JD02757, 1992,

Müller, J.-F. and Stavrakou, T.: Inversion of CO and NO_x emissions using the adjoint of the IMAGES model, Atmos. Chem. Phys., 5, 1157–1186, doi:10.5194/acp-5-1157-2005, 2005.

Murray, L. T., Jacob, D. J., Logan, J. A., Hudman, R. C., and Koshak, W. J.: Optimized regional and interannual variability of lightning in a global chemical transport model constrained by LIS/OTD satellite data, J. Geophys. Res., 117, D20307, doi:10.1029/2012JD017934, 2012.

Olivier, J. G. J. and J. J. M. Berdowski (2001) Global emissions sources and sinks, editex by: Berdowski, J., Guicherit, R., and Heij, B. J., The Climate System, 33–78, A.A. Balkema Publishers/Swets & Zeitlinger Publishers, Lisse, the Netherlands, ISBN 90 5809 255 0, 2001

Parrish, D. D. and Fehsenfeld, F. C.: Methods for gas-phase measurements of ozone, ozone precursors and aerosol precursors, Atmos. Environ., 34, 1921–1957, doi:10.1016/S1352-2310(99)00454-9, 2000.

Parton, W. J., Holland, E. A., Del Grosso, S. J., Hartman, M. D., Martin, R. E., Mosier, A. R., Ojima, D. S., and Schimel, D. S.: Generalized model for NO_x and N_2O emissions from soils, J. Geophys. Res.-Atmos., 106, 17403–17419, doi:10.1029/2001JD900101, 2001.

Potter, C., Matson, P., Vitousek, P., and Davidson, E.: Process modeling of controls on nitrogen trace gas emissions from soils worldwide, J. Geophys. Res.-Atmos., 101, 1361–1377, doi:10.1029/95JD02028, 1996.

Sauvage, B., Martin, R. V., van Donkelaar, A., and Ziemke, J. R.: Quantification of the factors controlling tropical tropospheric ozone and the South Atlantic maximum, J. Geophys. Res., 112, D11309, doi:10.1029/2006JD008008, 2007.

Scholes, M., Martin, R., Scholes, R., Parsons, D., and Winstead, E.: NO and N_2O emissions from savanna soils following the first simulated rains of the season, Nutr. Cycl. Agroecosys., 48, 115–122, doi:10.1023/A:1009781420199, 1997.

Schumann, U. and Huntrieser, H.: The global lightning-induced nitrogen oxides source, Atmos. Chem. Phys., 7, 3823–3907, doi:10.5194/acp-7-3823-2007, 2007.

Shepherd, M., Barzetti, S., and Hastie, D.: The production of atmospheric NO_x and N_2O from a fertilized agricultural soil, Atmos. Environ., 25, 1961–1969, doi:10.1016/0960-1686(91)90277-E, 1991.

Sneep, M., de Haan, J. F., Stammes, P., Wang, P., Vanbauce, C., Joiner, J., Vasilkov, A. P., and Levelt, P. F.: Three-way comparison between OMI and PARASOL cloud pressure products, J. Geophys. Res.-Atmos., 113, D15S23, doi:10.1029/2007JD008694, 2008.

Stavrakou, T., Müller, J.-F., Boersma, K. F., De Smedt, I., and van der A, R. J.: Assessing the distribution and growth rates of NO_x emission sources by inverting a 10 year record of NO_2 satellite columns, Geophys. Res. Lett., 35, L10801, doi:10.1029/2008GL033521, 2008.

Stavrakou, T., Müller, J.-F., Boersma, K. F., van der A, R. J., Kurokawa, J., Ohara, T., and Zhang, Q.: Key chemical NO_x sink uncertainties and how they influence top-down emissions of nitrogen oxides, Atmos. Chem. Phys., 13, 9057–9082, doi:10.5194/acp-13-9057-2013, 2013.

Stehfest, E. and Bouwman, L.: N_2O and NO emission from agricultural fields and soils under natural vegetation: summarizing available measurement data and modeling of global annual emissions, Nutr. Cycl. Agroecosys., 74, 207–228, doi:10.1007/s10705-006-9000-7, 2006.

Steinbacher, M., Zellweger, C., Schwarzenbach, B., Bugmann, S., Buchmann, B., Ordóñez, C., Prevot, A. S. H., and Hueglin, C.: Nitrogen oxide measurements at rural sites in Switzerland: Bias of conventional measurement techniques, J. Geophys. Res.-Atmos., 112, D11307, doi:10.1029/2006JD007971, 2007.

Steinkamp, J. and Lawrence, M. G.: Improvement and evaluation of simulated global biogenic soil NO emissions in an AC-GCM, Atmos. Chem. Phys., 11, 6063–6082, doi:10.5194/acp-11-6063-2011, 2011.

Steinkamp, J., Ganzeveld, L. N., Wilcke, W., and Lawrence, M. G.: Influence of modelled soil biogenic NO emissions on related trace gases and the atmospheric oxidizing efficiency, Atmos. Chem. Phys., 9, 2663–2677, doi:10.5194/acp-9-2663-2009, 2009.

Streets, D. G., Zhang, Q., Wang, L., He, K., Hao, J., Wu, Y., Tang, Y., and Carmichael, G. R.: Revisiting China's CO emissions after the Transport and Chemical Evolution over the Pacific (TRACE-P) mission: synthesis of inventories, atmospheric modeling, and observations, J. Geophys. Res.-Atmos., 111, D14306, doi:10.1029/2006JD007118, 2006.

Tørseth, K., Aas, W., Breivik, K., Fjæraa, A. M., Fiebig, M., Hjellbrekke, A. G., Lund Myhre, C., Solberg, S., and Yttri, K. E.: Introduction to the European Monitoring and Evaluation Programme (EMEP) and observed atmospheric composition change during 1972–2009, Atmos. Chem. Phys., 12, 5447–5481, doi:10.5194/acp-12-5447-2012, 2012.

Environmental Protection Agency (EPA): Technical assistance document for the chemiluminescence measurement of nitrogen dioxide, Tech. Rep., Environmental Monitoring and Support Laboratory, US Environmental Protection Agency, Research Triangle Park, NC 27711, EPA-600/4-75-003, 1975.

van der Werf, G. R., Randerson, J. T., Giglio, L., Collatz, G. J., Mu, M., Kasibhatla, P. S., Morton, D. C., DeFries, R. S., Jin, Y., and van Leeuwen, T. T.: Global fire emissions and the contribution of deforestation, savanna, forest, agricultural, and peat fires (1997–2009), Atmos. Chem. Phys., 10, 11707–11735, doi:10.5194/acp-10-11707-2010, 2010.

van Dijk, S. M., Gut, A., Kirkman, G. A., Gomes, B. M., Meixner, F. X., and Andreae, M. O.: Biogenic NO emissions from forest and pasture soils: Relating laboratory studies to field measurements, J. Geophys. Res.-Atmos., 107, LBA 25-1–LBA 25-11, doi:10.1029/2001JD000358, 2002.

van Donkelaar, A., Martin, R. V., Leaitch, W. R., Macdonald, A. M., Walker, T. W., Streets, D. G., Zhang, Q., Dunlea, E. J., Jimenez, J. L., Dibb, J. E., Huey, L. G., Weber, R., and Andreae, M. O.: Analysis of aircraft and satellite measurements from the Intercontinental Chemical Transport Experiment (INTEX-B) to quantify long-range transport of East Asian sulfur to Canada, Atmos. Chem. Phys., 8, 2999–3014, doi:10.5194/acp-8-2999-2008, 2008.

Vinken, G. C. M., Boersma, K. F., Jacob, D. J., and Meijer, E. W.: Accounting for non-linear chemistry of ship plumes in the GEOS-Chem global chemistry transport model, Atmos. Chem. Phys., 11, 11707–11722, doi:10.5194/acp-11-11707-2011, 2011.

Vinken, G. C. M., Boersma, K. F., van Donkelaar, A., and Zhang, L.: Constraints on ship NO_x emissions in Europe using GEOS-Chem and OMI satellite NO_2 observations, Atmos. Chem. Phys., 14, 1353–1369, doi:10.5194/acp-14-1353-2014, 2014.

Wang, Y., Jacob, D. J., and Logan, J.: Global simulation of tropospheric O_3-NO_x-hydrocarbon chemistry, 1. Model formulation, J. Geophys. Res., 130, 10713–10726, doi:10.1029/2004JD005237, 1998.

Wang, Y., McElroy, M. B., Martin, R. V., Streets, D. G., Zhang, Q., and Fu, T.-M.: Seasonal variability of NOx emissions over east China constrained by satellite observations: implications for combustion and microbial sources, J. Geophys. Res.-Atmos., 112, D06301, doi:10.1029/2006JD007538, 2007.

Williams, E. J., Parrish, D. D., Buhr, M. P., Fehsenfeld, F. C., and Fall, R.: Measurement of soil NO_x emissions in central Pennsylvania, J. Geophys. Res.-Atmos., 93, 9539–9546, doi:10.1029/JD093iD08p09539, 1988.

Yan, X., Ohara, T., and Akimoto, H.: Statistical modeling of global soil NO_x emissions, Global Biogeochem. Cy., 19, GB3019, doi:10.1029/2004GB002276, 2005.

Yang, W., Tan, B., Huang, D., Rautiainen, M., Shabanov, N., Wang, Y., Privette, J., Huemmrich, K., Fensholt, R., Sandholt, I., Weiss, M., Ahl, D., Gower, S., Nemani, R., Knyazikhin, Y., and Myneni, R.: MODIS leaf area index products: from validation to algorithm improvement, IEEE T. Geosci. Remote, 44, 1885–1898, doi:10.1109/TGRS.2006.871215, 2006.

Yevich, R. and Logan, J. A.: An assessment of biofuel use and burning of agricultural waste in the developing world, Global Biogeochem. Cy., 17, 1095, doi:10.1029/2002GB001952, 2003.

Yienger, J. J. and Levy, H.: Empirical model of global soil-biogenic NO_x emissions, J. Geophys. Res.-Atmos., 100, 11447–11464, doi:10.1029/95JD00370, 1995.

Zhang, L., Jacob, D. J., Knipping, E. M., Kumar, N., Munger, J. W., Carouge, C. C., van Donkelaar, A., Wang, Y. X., and Chen, D.: Nitrogen deposition to the United States: distribution, sources, and processes, Atmos. Chem. Phys., 12, 4539–4554, doi:10.5194/acp-12-4539-2012, 2012.

Zhao, C. and Wang, Y.: Assimilated inversion of NO_x emissions over east Asia using OMI NO_2 column measurements, Geophys. Res. Lett., 36, L06805, doi:10.1029/2008GL037123, 2009.

Table 1. Overview of total global 2005 NO_x emissions used in this study ($Tg\,N\,yr^{-1}$)[a]. Regional annual soil NO_x emissions are given, based on the Hudman et al. (2012) a priori (and applying the canopy reduction factor described in Sec. 2.1). These regions are identified in Sect. 3.1, and the region boundaries are given in Fig. 3 and Table S1.

Type	Total 2005	Inventory/Source
Anthropogenic	30	EDGAR/EMEP/NEI2005/CAC/BRAVO/Streets et al. (2006)
Aircraft	0.5	Baughcum et al. (1996)
Biofuel Burning	0.7	Yevich and Logan (2003)
Biomass Burning	4.8	Mu et al. (2011); van der Werf et al. (2010)
Lightning	5.8	Sauvage et al. (2007); Murray et al. (2012)
Soil (fertiliser)	9.6 (2.2)	Hudman et al. (2012)
– Argentina	0.32	
– Australia	0.05	
– Brazil	0.33	
– Eastern Europe	0.04	
– India	0.35	
– Midwestern USA	0.24	
– Namibia-Botswana	0.13	
– Sahel	0.44	
– South Kazakhstan	0.17	
– Spain-France	0.07	
– West-USA	0.10	
Total	51.4	

[a] $1\,Tg\,N = 3.29\,Tg\,NO_2$.

Table 2. β' values calculated by perturbing surface emissions in the 11 regions by 10 % (Eq. 3). Regions are as defined in Fig. 3 and Table S1. Unfiltered and annual averaged β' values are presented in the Supplementary Material.

Region	Jan	Feb	Mar	Apr	May	Jun	Jul	Aug	Sep	Oct	Nov	Dec
Argentina	2.2	2.1					2.0			2.1		
Australia	3.4	3.3	3.0	3.0	2.7	3.1						3.3
Brazil				2.3					2.1			
Eastern Europe[a]					2.5	2.8		2.4	2.3			
India			1.8		1.9	2.0					2.2	
Midwestern USA					2.1	2.6	2.4	2.4	2.0			
Namibia-Botswana		3.5		3.0					3.3		2.7	3.3
Sahel	2.0	2.1	2.0	2.1	2.2	2.3	2.4	2.4	2.3	2.0	2.1	2.5
South Kazakhstan					2.5		2.3					
Spain-France[a]					2.1	2.4						
West-USA					2.2			1.8	1.8	1.5		

[a] calculated for soil fraction larger than 0.2.

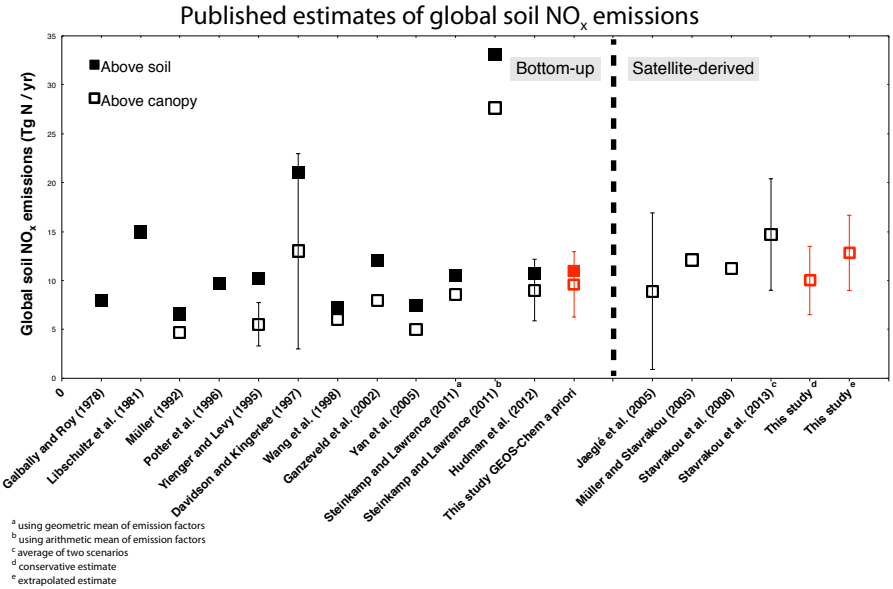

Figure 1. Summary of bottom-up and satellite-derived estimates of global soil NO_x emissions ($Tg\,N\,yr^{-1}$) reported in peer-reviewed literature. Open squares represent above-canopy global emissions, and solid squares represent above-soil global emissions (inventories used in this study are indicated by a red colour). Error bars are shown for studies reporting uncertainty estimates in above-canopy emissions.

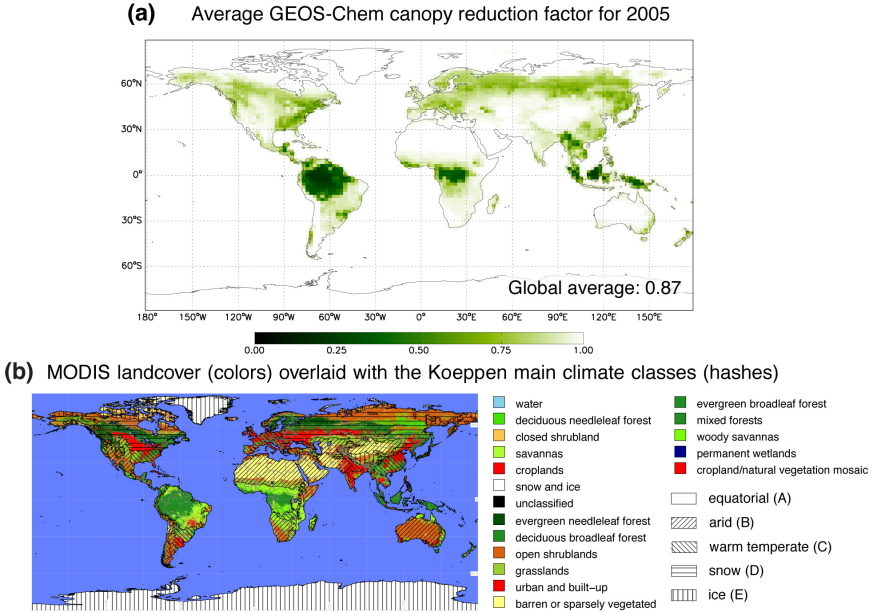

Figure 2. **(a)** Annual average of the canopy reduction factor (CRF) for 2005 in GEOS-Chem, calculated using the updated Jacob and Bakwin (1991) approach. **(b)** Köppen/MODIS climate classes, adapted from Steinkamp and Lawrence (2011).

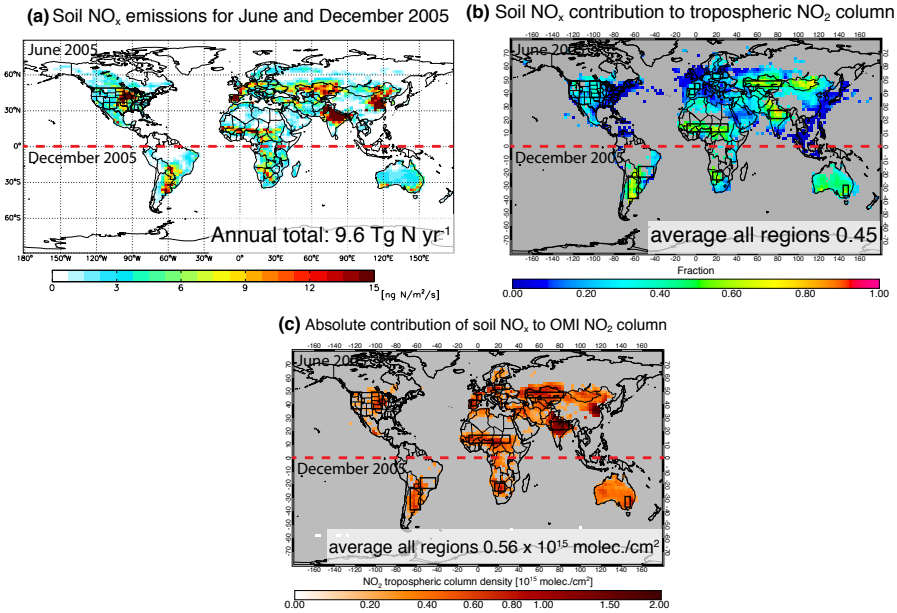

Figure 3. **(a)** Soil NO_x emissions for June (Northern Hemisphere) and December (Southern Hemisphere) 2005 used in the GEOS-Chem model (Hudman et al. (2012) and CRF of Jacob and Bakwin (1991), see Fig. 2a). **(b)** Contribution of soil NO_x emissions to the modelled tropospheric NO_2 column (λ_{soil}, calculated using Eq. 1) for June and December 2005. The 11 regions with high soil NO_2 column fractions used in this study are indicated with black rectangles (see Table S1 for latitude and longitude ranges of regions). **(c)** Estimated absolute contribution of soil NO_x emissions to the OMI NO_2 column for June and December 2005 (calculated by multiplying soil NO_2 column fractions with the OMI NO_2 column).

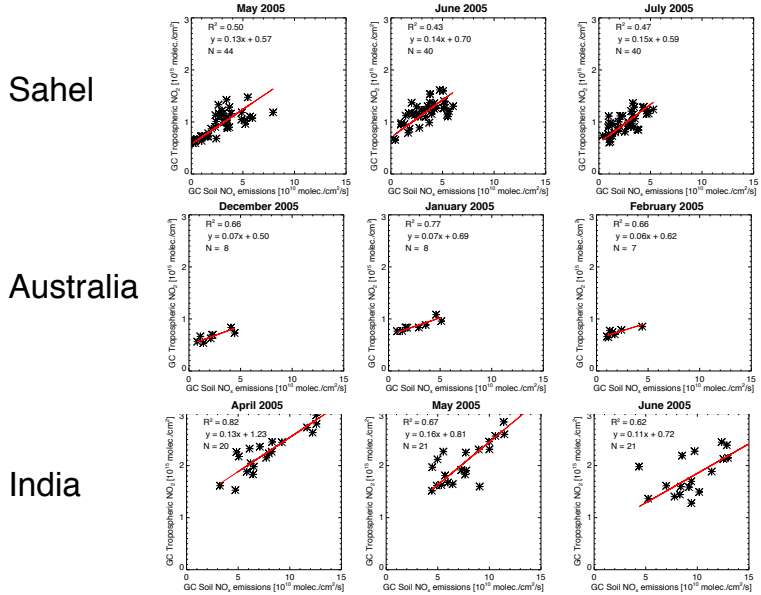

Figure 4. Relationship between monthly averaged soil NO_x emissions and tropospheric NO_2 columns for grid cells in the GEOS-Chem model ~~at~~ averaged between 13:00–15:00 LT after applying the filtering scheme of Sect. 3.1. Months with largest soil NO_x emissions are shown for the Sahel, Australia, and India (regions as defined in Fig. 3c and Table S1). Reduced Major Axis regression fit lines and statistics are shown, and statistics for all months (and other regions) are given in Table S1.

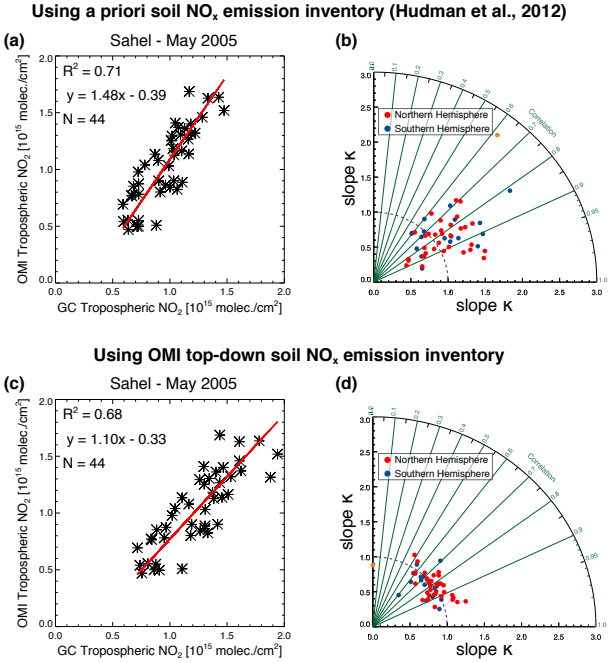

Figure 5. (a) Relationship between monthly averaged OMI and GEOS-Chem tropospheric NO_2 columns after applying the filtering scheme of Sect. 3.1 for the Sahel in May 2005 using a priori soil NO_x emissions in GEOS-Chem. Reduced Major Axis (RMA) regression fit line and statistics are shown. **(b)** Summary plot of RMA regression slopes and correlation coefficients for all months and regions (red dots for Northern Hemisphere, and blue dots for Southern Hemisphere) using a priori soil NO_x emissions in GEOS-Chem (values listed in Table S2). The orange dot represents South-Kazakhstan for May (see discussion in Sect. 4.2). **(c** and **d)** are similar to **(a** and **b)**, but modelled NO_2 columns now simulated using the OMI top-down soil NO_x inventory in GEOS-Chem (values of **(d)** listed in Table S3).

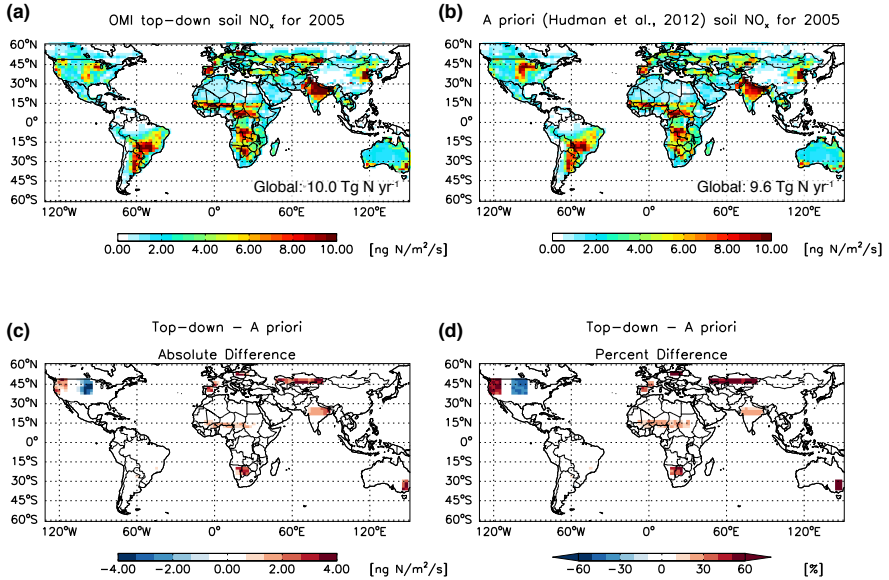

Figure 6. **(a)** Annual averaged OMI top-down soil NO_x emissions for 2005. **(b)** a priori soil NO_x emissions in the GEOS-Chem model for 2005 (Hudman et al. (2012) using the Jacob and Bakwin (1991) CRF). Absolute differences **(c)** and relative differences **(d)** between these annual averaged inventories are shown.

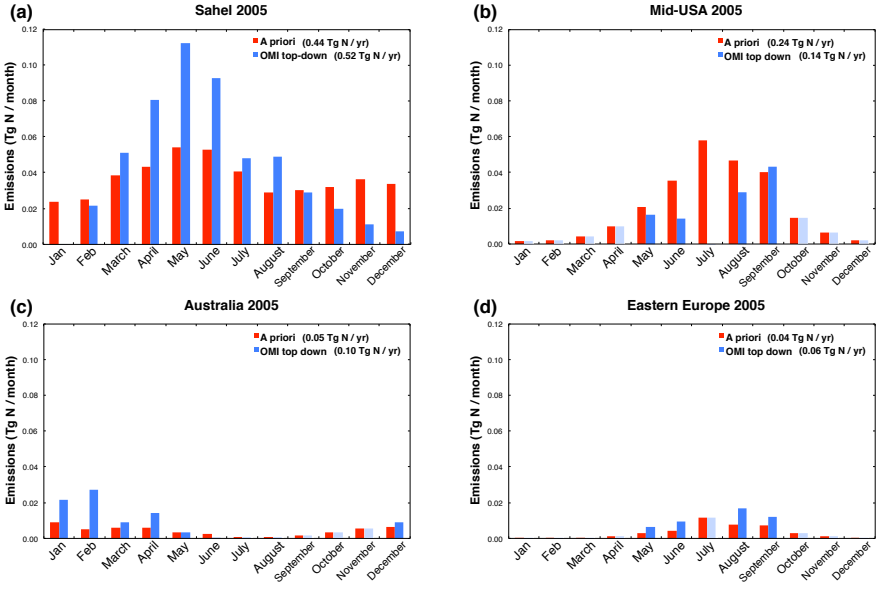

Figure 7. Monthly averaged soil NO_x emissions ($Tg\,N\,yr^{-1}$) in 2005 for the a priori inventory (Hudman et al., 2012, red), and the new OMI top-down inventory (blue, Fig. 6a) over: **(a)** Sahel, **(b)** Midwestern USA, **(c)** Australia, and **(d)** eastern Europe (areas as defined in Fig. 3 and Table S1). Light blue bars represent months for which no OMI top-down constraints were available, and top-down estimates adopt the bottom-up values.

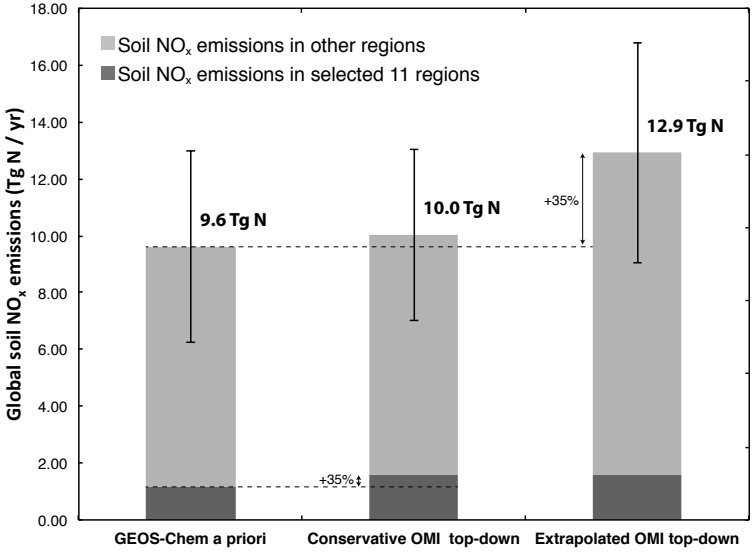

Figure 8. Global totals of soil NO_x emissions for 2005, with the 11-region total (regions indicated in Fig. 3) indicated by the dark grey colour (excluding the Midwestern USA in July, and South-Kazakhstan in May). Applying constraints to these 11 regions results in the conservative estimate for annual global soil NO_x emissions (middle bar). Extrapolating this increase of 35 % to all global soil NO_x emissions results in a total of 12.9 Tg N (right bar). Error bars are indicated as discussed in Sect. 4.4. Based on the discussions in Steinkamp and Lawrence (2011) and Hudman et al. (2012), we estimate the error in the a priori inventory at 35 % (based on uncertainties in emission factors, application of a CRF, and soil moisture).

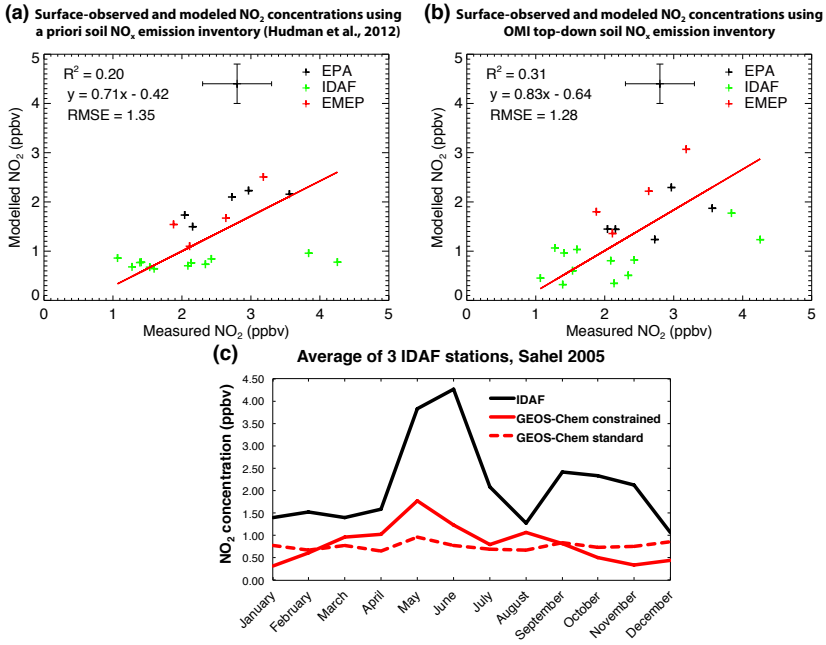

Figure 9. Relationship of monthly averaged surface-observed and modelled NO_2 concentrations, using the a priori soil NO_x emission inventory **(a)** and OMI top-down inventory **(b)**. Monthly averaged modelled and in-situ observed NO_2 concentrations are given for: Midwestern USA in black (observations from hourly EPA measurements), the Sahel in green (observations from monthly IDAF measurements), and Eastern Europe in red (observations from daily EMEP measurements, see Fig. S1 for locations of all measurement stations). Reduced Major Axis regression fit lines and statistics are shown, and typical error bars are indicated (see Sect. 4.3). The seasonal cycle of NO_2 concentrations in the Sahel is given in **(c)** for IDAF surface measurements (red), GEOS-Chem simulated NO_2 concentrations using the OMI top-down soil NO_x inventory (black), and simulated concentrations using the a priori inventory (black dashed line).